ACS APPLIED MATERIALS & INTERFACES

Research Article

www.acsami.org

Observation and Mediation of the Presence of Metallic Lead in Organic–Inorganic Perovskite Films

Golnaz Sadoughi,[†] David E. Starr,[‡] Evelyn Handick,[‡] Samuel D. Stranks,[†] Mihaela Gorgoi,[§] Regan G. Wilks,[‡,∥] Marcus Bär,*[,‡,∥,⊥] and Henry J. Snaith*[,†]

[†]Clarendon Laboratory, Department of Physics, University of Oxford, Parks Road, Oxford OX1 3PU, United Kingdom

[‡]Renewable Energy, Helmholtz-Zentrum Berlin für Materialien und Energie GmbH, Hahn-Meitner-Platz 1, 14109 Berlin, Germany

[§]Methods and Instrumentation for Synchrotron Radiation Research, Helmholtz-Zentrum Berlin für Materialien und Energie GmbH, Albert-Einstein-Strasse 15, 12489 Berlin, Germany

[∥]Energy Materials In-Situ Laboratory (EMIL), Helmholtz-Zentrum Berlin für Materialien und Energie GmbH, Albert-Einstein-Strasse 15, 12489 Berlin, Germany

[⊥]Institut für Physik und Chemie, Brandenburgische Technische Universität Cottbus-Senftenberg, Platz der Deutschen Einheit 1, 03046 Cottbus, Germany

Supporting Information

ABSTRACT: We have employed soft and hard X-ray photoelectron spectroscopies to study the depth-dependent chemical composition of mixed-halide perovskite thin films used in high-performance solar cells. We detect substantial amounts of metallic lead in the perovskite films, which correlate with significant density of states above the valence band maximum. The metallic lead content is higher in the bulk of the perovskite films than at the surface. Using an optimized postanneal process in air, we can reduce the metallic lead content in the perovskite film. This process reduces the amount of metallic lead and a corresponding increase in the photoluminescence quantum efficiency of the perovskite films can be observed. This correlation indicates that metallic lead impurities are likely a key defect whose concentration can be controlled by simple annealing procedures in order to increase the performance for perovskite solar cells.

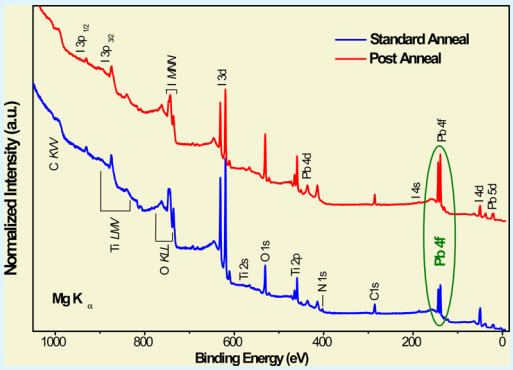

KEYWORDS: *perovskite solar cell, methylammonium lead iodide chloride, metallic lead, XPS, PLQE*

INTRODUCTION

Recent dramatic increases in power conversion efficiencies have stimulated large research efforts in the use of organic–inorganic perovskites for high performance hybrid solar cells.[1−3] In just a few years, power conversion efficiencies have increased from 3.8% in 2009[4] to greater than 20% in 2014,[5] with high levels of performance reported for numerous device configurations. The highest performing devices have consisted of active layers of either a thin mesoporous TiO_2 layer sensitized with a methylammonium lead trihalide perovskite ($MAPbX_3$, where X is I, Cl, Br, or mixtures thereof) and capped with a layer of solid perovskite,[6,7] a mesoporous insulating scaffold capped with a solid perovskite absorbing layer,[8,9] or a simple solid perovskite layer in a planar heterojunction configuration.[10,11] Beyond solar cell applications, these organic–inorganic perovskites have also shown promise for use in light-emitting diodes[12] and lasers.[13,14]

Despite extensive research, there are few detailed reports correlating the chemical and electronic structures of the perovskite layer. Using HAXPES (hard X-rays photoelectron spectroscopy), XPS (X-ray photoelectron spectroscopy), and EPR (continuous-wave electron paramagnetic resonance) spectroscopy Lindblad et al., B. Conings et al., and I. Shkrob et al., respectively, have shown the presence of metallic lead in perovskite films.[15−17] The presence of metallic lead could negatively impact the device performance by, for example, providing nonradiative decay pathways and/or forming shunt paths. We have recently reported evidence of sub-band gap electronic trap states and demonstrated their detrimental impact on device performance.[18,19] Although these sub-band gap states may not be solely attributed to metallic lead, understanding and reducing the number of these states will be crucial for further optoelectronic device improvement.

In this work, we use synchrotron-based hard X-ray photoelectron spectroscopy (HAXPES), lab-based soft X-ray (Mg K_α) photoelectron spectroscopy (XPS), and photoluminescence quantum efficiency (PLQE) measurements to study the effects of various annealing treatments on mixed-halide, organic–inorganic perovskite films. We find that following a standard perovskite layer preparation, a substantial

Received: March 17, 2015
Accepted: May 19, 2015
Published: May 19, 2015

DOI: 10.1021/acsami.5b02237
ACS Appl. Mater. Interfaces 2015, 7, 13440−13444

amount of metallic lead is present in the films. Simultaneously, we can identify significant density of states above the perovskite valence band maximum. By subjecting the films to a postannealing process in air, the intensity of the photoemission signals from metallic lead and the states above the valence band maximum is substantially reduced, and the PLQE increases. This work demonstrates the importance of understanding and controlling the annealing processes used in perovskite film preparation and establishes a protocol for producing higher-quality perovskite films that could lead to improved optoelectronic performance.

EXPERIMENTAL SECTION

Sample Preparation. The synthesis of the perovskite $CH_3NH_3PbI_{3-x}Cl_x$ has been reported elsewhere.[6] Briefly, to make the $CH_3NH_3PbI_{3-x}Cl_x$ precursor solution, we dissolved methylammonium iodide and lead(II) chloride (respectively 3:1 molar ratio) in anhydrous *N*,*N*-dimethylformamide (DMF) to final concentrations of 0.88 M lead chloride and 2.64 M methylammonium iodide. To make perovskite layers with different thicknesses, we diluted the precursor solution in DMF.

Perovskite layers for all measurements were fabricated on either TiO_2-coated fluorine-doped tin oxide (FTO) substrates (Pilkington, TEC7) or glass. Layers of compact TiO_2 were deposited by spin-coating an acidic solution of titanium isopropoxide in ethanol at 2000 rpm for 60 s, drying at 150 °C, and then annealing at 500 °C for 45 min.

The perovskite layers were deposited by spin-coating a $CH_3NH_3PbI_{3-x}Cl_x$ precursor solution at 2000 rpm in a nitrogen filled glovebox for 45 s. After spin-coating, the films were left to dry at room temperature in the glovebox for 30 min to allow slow solvent evaporation. They were then annealed to crystallize the perovskite in the glovebox at 90 °C for 2.5 h. This procedure is referred to as standard annealing in the Results and Discussion section. Some samples went through further annealing in air at 70 °C for different length of times ranging from 10 min to 14 h.

Between preparation and measurements, the sample exposure to ambient conditions was minimized. To prevent excess exposure of the perovskite films to moisture, they were packed and transported in a dry environment and stored in a N_2 purged glovebox for soft and hard X-ray photoelectron spectroscopy measurements. For PLQE measurements the perovskite films were protected by spin-coating a layer of the insulating polymer poly(methyl methacrylate) (PMMA; Sigma-Aldrich, 10 mg/mL) on top of the film.

Hard X-ray Photoelectron Spectroscopy. Hard X-ray photoelectron spectroscopy (HAXPES) experiments were conducted at the HiKE end-station on the KMC-1 beamline of the BESSY-II electron storage ring.[20,21] This end-station is equipped with a Scienta R4000 electron energy analyzer capable of measuring photoelectron kinetic energies up to 10 keV. A pass energy of 200 eV was used for all measurements. Spectra were recorded using photon energies of approximately 2 and 6 keV with the Si(111) and Si(422) crystals of a double crystal monochromator providing a beamline resolution of approximately 0.2 eV at both photon energies resulting in a combined analyzer plus beamline resolution of approximately 0.25 eV. The top surface of the sample was grounded for all measurements. The binding energy was calibrated by measuring the 4f spectrum of a grounded Au foil and setting the Au $4f_{7/2}$ binding energy equal to 84.00 eV. Since the inelastic mean free paths (IMFP) of electrons of different kinetic energies through lead halide-based perovskite materials are not known, we estimate it to be similar to that in PbI_2. In that case, the IMFP for Pb 4f photoelectrons excited with 6 keV is 9.8 nm[22,23] and thus approximately 3 (4) times greater than when using 2 keV (Mg K_α: 1253.56 eV).

The valence band spectra have been normalized by the intensity of the main peak in the spectrum at approximately 2.5 eV. These states have recently been attributed to either predominantly I 5p,[15] or Pb 6s and I 5p hybridized states.[24]

Lab-Based soft X-ray Photoelectron Spectroscopy. XPS measurements were conducted using Mg K_α (1253.56 eV) radiation and a SPECS PHOIBOS 150 MCD electron energy analyzer. The electron energy analyzer was calibrated according to D. Briggs et al.[25] For the collection of the survey spectra and the I 4d and Pb 4f detail spectra, the pass energies were 50 and 30 eV, respectively.

Photoluminescence Quantum Efficiency Measurement. Photoluminescence quantum efficiency (PLQE) measurements were taken in an integrating sphere using established techniques.[26] The samples were photoexcited using a 532 nm CW laser operating at a fluence of 200 mW/cm^2 (equivalent to ~3 suns).

RESULTS AND DISCUSSION

In Figure 1, we show Pb 4f detail spectra recorded with photon excitation energies of 2 and 6 keV for the two types of sample

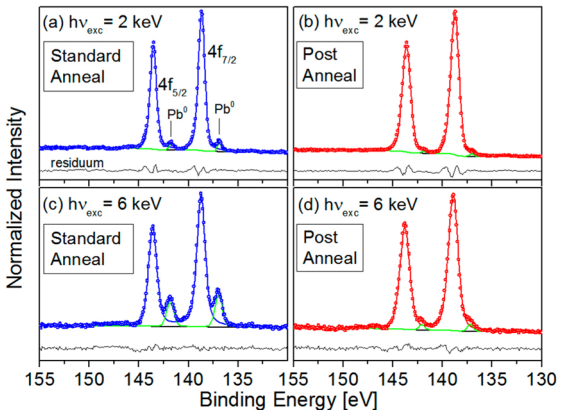

Figure 1. Pb $4f_{5/2}$ and $4f_{7/2}$ detail spectra (dots), using excitation photon energies of (a, b) 2 and (c, d) 6 keV, of a 60 nm thick $CH_3NH_3PbI_{3-x}Cl_x$ perovskite film on TiO_2 subject to two different sample annealing treatments: Standard (a, c) annealed and (b, d) post-annealed. The samples for spectra a and c underwent a standard annealing treatment in N_2-atmosphere of 90 °C for 150 min while the samples for spectra b and d have undergone further annealing in air at 70 °C for 14 h. The fits and respective residua (solid lines) are also shown. Satellite contributions (see the Supporting Information, Figure S1) to the spectra have been subtracted.

treatments: standard annealing and postannealing for 14 h (see Experimental Section for details about sample preparation and annealing procedures). Because the inelastic mean free path of the photoelectrons (and thus the information depth of the measurement) generally increases with increasing photoelectron kinetic energy, the spectra taken with 2 keV photon excitation are primarily characteristic of the surface region of the perovskite film while the 6 keV-excited spectra have a larger relative bulk component. For example, the inelastic mean free path for Pb 4f photoelectrons in PbI_2 is approximately 3.8 and 9.7 nm for spectra taken with 2 and 6 keV photon energies, respectively.[23] The Pb 4f spectrum consists of two separate contributions: $4f_{7/2}$ and $4f_{5/2}$ peaks with a spin−orbit splitting of 4.9 eV. The largest Pb $4f_{7/2}$ peak in all spectra is found at 138.7 eV, consistent with the Pb $4_{f7/2}$ binding energies of lead-halides (PbI_2, $PbCl_2$, and $PbBr_2$) and is attributed to Pb in the perovskite structure.[15,27,28] A smaller Pb $4f_{7/2}$ peak is observed in all spectra at a binding energy (137.0 eV) consistent with metallic lead (Pb^0).[16,29,30] This low-binding energy Pb $4f_{7/2}$ contribution is smaller for the post annealed than for the standard annealed samples and for the measurements with 2 keV than with 6 keV excitation energy. This indicates that the relative concentration of metallic Pb is higher in the bulk than

DOI: 10.1021/acsami.5b02237
ACS Appl. Mater. Interfaces 2015, 7, 13440−13444

near the surface of the perovskite film and that annealing the sample reduces the relative amount of metallic Pb both at the surface and in the bulk. Note that the Pb $4f_{7/2}$ binding energy of Pb in both PbO and PbO_2 is approximately 137.7 eV,[31] and thus we cannot entirely exclude the possible presence of Pb-oxide in our samples. However, each branch (i.e., $4f_{7/2}$ and $4f_{5/2}$) in our spectra can be adequately fitted with two main Pb 4f peaks attributable to Pb in the perovskite structure and metallic Pb. By accurately fitting the spectra we can quantify the relative contributions of photoemission signals from metallic Pb and from Pb in the perovskite structure and their changes upon annealing. To do so, the complex satellite features, extending more than 20 eV to higher binding energy beyond the main peaks, must be taken into account (see the Supporting Information). These satellite features are due to electron (kinetic) energy losses that have been attributed to transitions between the valence and conduction bands in Pb(II) halides.[27]

Quantification of the Pb 4f spectral contributions in Figure 1 reveals that the fraction of the metallic Pb signal for the standard annealed samples is 0.15 for the 6 keV photon energy spectrum and 0.03 for the 2 keV spectrum. After postannealing, the metallic Pb signal fraction is reduced to approximately 0.03 and 0.01 for the 6 and 2 keV spectra, respectively, demonstrating that postannealing reduces the amount of metallic Pb in both the bulk and surface regions of the perovskite film (see Figure 1b, d). The fraction of metallic Pb in the bulk is reduced more than in the surface region, i.e., by a factor of 5 compared to a factor of 3, suggesting that the decrease in metallic Pb is most likely due to further incorporation of Pb into the perovskite structure. The lack of any new peaks appearing at 137.7 eV in the Pb 4f spectra, which we would expect if there was formation of significant amounts of Pb-oxide species with annealing, support this model. We do note, however, that the perovskite crystal is likely to be permeable to oxygen, and we cannot conclusively rule out the formation of small amounts of PbO or PbO_2 upon annealing. Please note that not all samples studied exhibited the same metallic Pb contribution. However, when observed, the fraction of metallic Pb was always higher in the bulk of the perovskite film than in the surface region.

In addition to a decrease in the amount of metallic Pb, we observe a slight increase in the Ti and O signals upon annealing, likely associated with dewetting of the TiO_2 substrate (see the Supporting Information). We also observe a decrease in the I to Pb ratio in the surface region of the sample after annealing (see the Supporting Information). Lindblad et al. made similar observations, which they correlate with an increase in the amount of metallic Pb in the sample. This would appear to be in contradiction to our results—the decreased I to Pb ratio correlates with a decrease in metallic Pb—however, the inconsistency between these two results may be due to the fact that our estimates of the I to Pb ratio are based on much more surface sensitive measurements than those of Lindblad et al., and that our perovskites are formed from a 3 to 1 mixture of MAI to $PbCl_2$ whereas Lindblad et al. used a 1 to 1 mixture of PbI_2 and MAI (i.e., a pure iodine perovskite). Because Cl_2 is a gas at ambient conditions, whereas I_2 is a solid, the halogen content of the two samples may not correlate in the same way with the amount of metallic Pb; particularly if the metallic Pb is formed by initial dissociation of the lead halide (which would presumably be more likely to occur in a Cl-containing sample). We have recently shown that there is also an inhomogeneous chlorine distribution in $CH_3NH_3PbI_{3-x}Cl_x$ layers; the surface is void of any significant amount of chlorine, it is present in higher quantities toward the $CH_3NH_3PbI_{3-x}Cl_x/TiO_2$ interface.[32] Whether this is related to the here reported increased formation of metallic lead in the bulk of $CH_3NH_3PbI_{3-x}Cl_x$ layers is currently not clear.

Figure 2 shows valence band spectra for a 60 nm thick $CH_3NH_3PbI_{3-x}Cl_x$ perovskite film on TiO_2 with standard

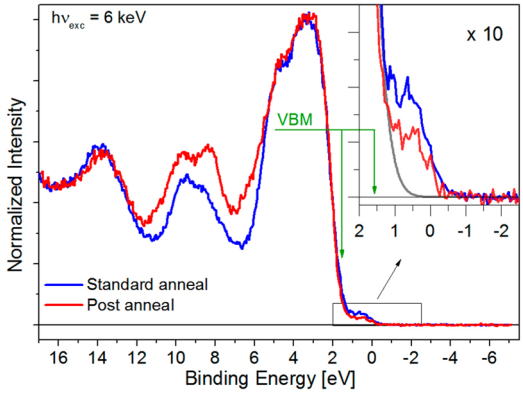

Figure 2. Valence band spectra with 6 keV excitation of a 60 nm thick $CH_3NH_3PbI_{3-x}Cl_x$ perovskite film on TiO_2 following two different sample treatments; a standard anneal (blue spectrum) and a further post anneal (red spectrum). The inset shows an expansion (10× magnification) of the region around the Fermi level at a binding energy of 0 eV to highlight the change in density of states above the valence band maximum (VBM, marked with green arrows). The gray line represents the fit of the valence band onset with a Voigt profile as a reference for a spectrum with no density of states above VBM.

annealing (blue) and postannealing (red) measured with photon excitation energy of 6 keV. Previous photoemission studies of $CH_3NH_3PbI_3$ perovskite films comparing measured spectra to density functional theory calculations of model compounds, allow a description of the valence band spectra in terms of the relative contributions of the composite elements.[18] The spectral region from approximately 2−6 eV is attributed to predominantly Pb 6s and I 5p hybridized states.[15] From approximately 6−12 eV, the density of states is dominated by carbon and nitrogen of the methylammonium cation,[15] however, due to their much lower photoionization cross sections for the employed excitation energies, these states contribute little to the measured valence band spectra, and thus we ascribe the observed density of states in that region mainly to contributions from the TiO_2 substrate. The O 2p derived substrate features at approximately 8 eV increase in intensity upon postannealing (red spectrum), which may be due to dewetting of the perovskite films upon the TiO_2 substrate (see the Supporting Information). The VBM position of the $CH_3NH_3PbI_{3-x}Cl_x$ perovskite film was derived by linear approximation of the leading valence band edge to be 1.54 eV (±0.10 eV) below the Fermi level, as indicated in Figure 2 and is in agreement with reported VBM values in literature.[33]

In the inset of Figure 2, we have highlighted the presence of states between the valence band maximum and the Fermi level. Similar to the Pb 4f peaks associated with metallic Pb, the intensity of this signal decreases upon postannealing. The difficulty and uncertainty associated with quantifying spectral features in the valence band region however precludes a direct quantitative correlation between the amount of metallic Pb and the density of states near the Fermi level.

DOI: 10.1021/acsami.5b02237
ACS Appl. Mater. Interfaces 2015, 7, 13440−13444

To attempt to understand the effects of the changing composition and electronic structure on solar cell device performance, we use photoluminescence quantum efficiency (PLQE). Figure 3 shows the PLQE signal at 532 nm of

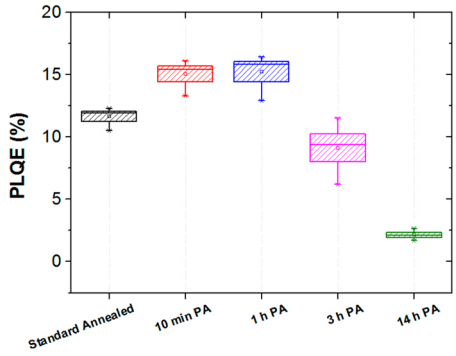

Figure 3. Photoluminescence quantum efficiency (PLQE) measurements of $CH_3NH_3PbI_{3-x}Cl_x$ films on glass capped with a thin PMMA layer after a standard anneal in comparison to different postannealing (PA) treatments in air.

similarly prepared $CH_3NH_3PbI_{3-x}Cl_x$ perovskite films on TiO_2 coated glass before and after postannealing (PA) treatments of different durations (up to 14 h) at 70 °C in air. For PAs up to 1 h, we see an improvement in PLQE. This improvement is consistent with the expected effect of reducing the amount of metallic lead, which could be detrimental to the PLQE either by introducing shunt paths and/or by forming sub-band gap states that would act as nonradiative decay pathways.[15,18,19] When we anneal the perovskite in air for 3 h or longer the PLQE decreases, which is likely due to degradation of the perovskite film via loss of the organic component and the formation of PbI_2.[34−36] We note that the defect chemistry in the perovskite material is likely to be complicated, with many different defect species present. Although we have shown here that overannealing the sample can reduce the metallic lead content, it also drives the perovskite material toward degradation,[37] which could result in significant nonstoichiometry potentially inducing nonradiative recombination sites (unrelated to metallic Pb). The optimum postannealing conditions therefore appear to be approximately 1 h at 70 °C. This is consistent with previous studies on the light-emitting properties of perovskite films, where crystallization in air has shown to deliver perovskite films with higher emissivity than crystallization in nitrogen.[13] In general, these results highlight the importance of understanding the nature of defects and their correlation with subgap states and provide a means to control their concentration. Such studies are a basis for a cognitive approach to optimizing the performance of perovskite-based optoelectronic devices via controlled postannealing.

CONCLUSION

In summary, we have studied the chemical composition of perovskite thin films before and after postannealing in air using soft and hard X-ray photoelectron spectroscopies. We show that metallic Pb is present in the perovskite layer and that its concentration relative to that of the Pb in the perovskite structure is higher in the bulk of the film than at its surface. Post annealing in air reduces the metallic lead content of the perovskite layers. Further, we have correlated the concentration of metallic Pb with the density of states above the valence band maximum and close to the Fermi level. Reducing the metallic Pb content reduces this density of states and correlates with an improvement of the photoluminescence quantum efficiency of the films. This work demonstrates the importance of understanding which impurities or defects have a detrimental impact upon the photovoltaic performance of the perovskite material and establishing a means to control their concentration.

ASSOCIATED CONTENT

Supporting Information

Figures S-1−S-5. The Supporting Information is available free of charge on the ACS Publications website at DOI: 10.1021/acsami.5b02237.

AUTHOR INFORMATION

Corresponding Authors

*E-mail: marcus.baer@helmholtz-berlin.de.
*E-mail: h.snaith1@physics.ox.ac.uk.

Notes

The authors declare no competing financial interest.

ACKNOWLEDGMENTS

This work was part funded by the Engineering and Physical Sciences Research Council (EPSRC). Part of the research leading to the results has also received funding from the European Union Seventh Framework Program [FP7/2007-2013] under grant agreement number 604032 of the MESO project. D.E.S., E.H., R.G.W., and M.B acknowledge funding by the Impuls- und Vernetzungsfonds of the Helmholtz Association (VH-NG-423).

REFERENCES

(1) Green, M. a.; Ho-Baillie, A.; Snaith, H. J. The Emergence of Perovskite Solar Cells. *Nat. Photonics* **2014**, *8*, 506−514.
(2) Kazim, S.; Nazeeruddin, M. K.; Grätzel, M.; Ahmad, S. Perovskite as Light Harvester: a Game Changer in Photovoltaics. *Angew. Chem., Int. Ed.* **2014**, *53*, 2812−2824.
(3) Boix, P. P.; Nonomura, K.; Mathews, N.; Mhaisalkar, S. G. Current Progress and Future Perspectives for Organic/Inorganic Perovskite Solar Cells. *Mater. Today.* **2014**, *17*, 16−23.
(4) Kojima, A.; Teshima, K.; Shirai, Y.; Miyasaka, T. Organometal Halide Perovskites as Visible-Light Sensitizers for Photovoltaic. *J. Am. Chem. Soc.* **2009**, *131*, 6050−6051.
(5) National Renewable Energy Laboratory, *Best Research Cell Efficiencies Chart*; http://www.nrel.gov/ncpv/images/efficiency_chart.jpg, April 2015.
(6) Lee, M. M.; Teuscher, J.; Miyasaka, T.; Murakami, T. N.; Snaith, H. J. Efficient Hybrid Solar Cells Based on Meso-Superstructured Organometal Halide Perovskites. *Science* **2012**, *338*, 643−647.
(7) Jeon, N. J.; Noh, J. H.; Kim, Y. C.; Yang, W. S.; Ryu, S.; Seok, S. Il. Solvent Engineering for High-Performance Inorganic−Organic Hybrid Perovskite Solar Cells. *Nat. Mater.* **2014**, *13*, 897−903.
(8) Wang, J. T.; Ball, J. M.; Barea, E. M.; Abate, A.; Alexander-webber, J. A.; Huang, J.; Saliba, M.; Mora-sero, I.; Bisquert, J.; Snaith, H. J.; Nicholas, R. J. Low-Temperature Processed Electron Collection Layers of Graphene/ TiO_2 Nanocomposites in Thin Film Perovskite Solar Cells. *Nano Lett.* **2014**, *14*, 724−730.
(9) Wojciechowski, K.; Saliba, M.; Leijtens, T.; Abate, A.; Snaith, H. J. Sub-150°C Processed Meso-Superstructured Perovskite Solar Cells with Enhanced Efficiency. *Energy Environ. Sci.* **2014**, *7*, 1142−1147.
(10) Eperon, G. E.; Burlakov, V. M.; Docampo, P.; Goriely, A.; Snaith, H. J. Morphological Control for High Performance Solution-Processed Planar Heterojunction Perovskite Solar Cells. *Adv. Funct. Mater.* **2014**, *24*, 151−157.

DOI: 10.1021/acsami.5b02237
ACS Appl. Mater. Interfaces 2015, 7, 13440−13444

(11) Zhou, H.; Chen, Q.; Li, G.; Luo, S.; Song, T.; Duan, H. S.; Hong, Z.; You, J.; Liu, Y.; Yang, Y. Interface Engineering of Highly Efficient Perovskite Solar Cells. *Science* **2014**, *1*, 542−546.
(12) Tan, Z. K.; Moghaddam, R. S.; Lai, M. L.; Docampo, P.; Higler, R.; Deschler, F.; Price, M.; Sadhanala, A.; Pazos, L. M.; Credgington, D.; Hanusch, F.; Bein, T.; Snaith, H. J.; Friend, R. H. Bright Light-Emitting Diodes Based on Organometal Halide Perovskite. *Nat. Nanotechnol.* **2014**, *9*, 687−692.
(13) Deschler, F.; Price, M.; Pathak, S.; Klintberg, L. E.; Jarausch, D.; Higler, R.; Hu, S.; Leijtens, T.; Stranks, S. D.; Snaith, H. J.; Atatu, M.; Phillips, R. T.; Friend, R. H. High Photoluminescence Efficiency and Optically Pumped Lasing in Solution-Processed Mixed Halide Perovskite Semiconductors. *J. Phys. Chem. Lett.* **2014**, *5*, 1421−1426.
(14) Xing, G.; Mathews, N.; Lim, S. S.; Yantara, N.; Liu, X.; Sabba, D.; Grätzel, M.; Mhaisalkar, S.; Sum, T. C. Low-Temperature Solution-Processed Wavelength-Tunable Perovskites for Lasing. *Nat. Mater.* **2014**, *13*, 476−480.
(15) Lindblad, R.; Bi, D.; Park, B.; Oscarsson, J.; Gorgoi, M.; Siegbahn, H.; Odelius, M.; Johansson, E. M. J.; Rensmo, H. Electronic Structure of TiO_2 /$CH_3NH_3PbI_3$ Perovskite Solar Cell Interfaces. *J. Phys. Chem. Lett.* **2014**, *5*, 648−653.
(16) Conings, B.; Baeten, L.; De Dobbelaere, C.; D'Haen, J.; Manca, J.; Boyen, H. G. Perovskite-Based Hybrid Solar Cells Exceeding 10% Efficiency with High reproducibility Using a Thin Film Sandwich Approach. *Adv. Mater.* **2014**, *26*, 2041−2046.
(17) Shkrob, I. A.; Marin, T. W. Charge Trapping in Photovoltaically Active Perovskites and Related Halogenoplumbate Compounds. *J. Phys. Chem. Lett.* **2014**, *5*, 1066−1071.
(18) Leijtens, T.; Stranks, S. D.; Eperon, G. E.; Lindblad, R.; Johansson, E. M. J.; Ball, J. M.; Lee, M. M.; Snaith, H. J.; Mcpherson, I. J. Electronic Properties of Meso-Superstructured and Planar Organometal Halide Perovskite Films: Charge Trapping, Photodoping, and Carrier Mobility. *ACS Nano* **2014**, *8*, 7147−7155.
(19) Stranks, S. D.; Burlakov, V. M.; Leijtens, T.; Ball, J. M.; Goriely, A.; Snaith, H. J. Recombination Kinetics in Organic-Inorganic Perovskites: Excitons, Free Charge, and Subgap States. *Phys. Rev. Appl.* **2014**, *2*, 034007.
(20) Gorgoi, M.; Svensson, S.; Schafers, F.; Ohrwall, G.; Mertin, M.; Bressler, P.; Karis, O.; Siegbahn, H.; Sandell, A.; Rensmo, H.; Doherty, W.; Jung, C.; Braun, W.; Eberhardt, W. The High Kinetic Energy Photoelectron Spectroscopy Facility at BESSY Progress and First Results. *Nucl. Instrum. Methods Phys. Res., Sect. A* **2009**, *601*, 48−53.
(21) Schaefers, F.; Mertin, M.; Gorgoi, M. KMC-1: A High Resolution and High Flux Soft X-Ray Beamline at BESSY. *Rev. Sci. Instrum.* **2007**, *78*, 123102.
(22) http://www.nist.gov/srd/onlinelist.cfm.
(23) Tanuma, S.; Powell, C. J.; Penn, D. R. Calculations of Electron Inelastic Mean Free Paths. *Surf. Interface Anal.* **1993**, *21*, 165−176.
(24) Even, J.; Pedesseau, L.; Jancu, J.; Katan, C. Importance of Spin−Orbit Coupling in Hybrid Organic/Inorganic Perovskites for Photovoltaic Applications. *J. Phys. Chem. Lett.* **2013**, *4*, 2999−3005.
(25) Briggs, D.; Seah, M. P. *Auger and X-ray Photoelectron Spectroscopy, Practical Surface Analysis*; Wiley: New York, 1990.
(26) Mello, J. C.; Wittmann, H. F.; Friend, R. H. An Improved Experimental Determination of External Photoluminescence Quantum Efficiency. *Adv. Mater.* **1997**, *9*, 230−232.
(27) Scrocco, M. X-Ray Photoemission Spectra of Pb(II) Halides: A Study of the Satellites on the Core and Valence Bands. *Phys. Rev. B* **1982**, *25*, 1535.
(28) Moulder, J.; Stickle, W.; Sobol, P.; Bomben, K. *Handbook of X-Ray Photoelectron Spectroscopy*. Phys. Electron. Div.: Eden Prairie, 1995.
(29) Hinnen, C.; Huong, C. N. van; Marcus, P. A Comparative X-Ray Photoemission Study of $Bi_2Sr_2CaCu_2O_{8+\delta}$ and $Bi_{1.6}Pb_{0.4}Sr_2CaCu_2O_{8+\delta}$. *J. Electron Spectrosc. Relat. Phenom.* **1995**, *73*, 293−304.
(30) Wagner, C. D.; Taylor, J. A. Generation of XPS Auger Lines by Bremsstrahlung. *J. Electron Spectrosc. Relat. Phenom.* **1980**, *20*, 83−93.
(31) Wagner, C. D.; Riggs, W. M.; Davis, L. E.; Moulder, J. F.; Muilenberg, G. E. *Handbook of X-ray Photoelectron Spectroscopy* Perkin-Elmer Corp. Physical Electronics Division: Eden Prairie, MN, 1979.
(32) Starr, D. E.; Sadoughi, G.; Handick, E.; Wilks, R. G.; Alsmeier, J. H.; Köhler, L.; Gorgoi, M.; Snaith, H. S.; Bar, M. Direct Observation of an Inhomogeneous Chlorine Distribution in $CH_3NH_3PbI_{3-x}Cl_x$ Layers: Surface Depletion and Interface Enrichment. *Energy Environ. Sci.* **2015**, *8*, 1609−1615.
(33) Miller, E. M.; Zhao, Y.; Mercado, C.; Saha, S.; Luther, J. M.; Zhu, K.; Stevanovic, V.; Perkins, C. L.; van de Lagemaat. Substrate-Controlled Band Positions in $CH_3NH_3PbI_3$ Perovskite Films. *J. Phys. Chem. Chem. Phys.* **2014**, 22122−22130.
(34) Noh, J. H.; Im, S. H.; Heo, J. H.; Mandal, T. N.; Seok, S. Il. Chemical Management for Colorful, Efficient, and Stable Inorganic−Organic Hybrid Nanostructured Solar Cells. *Nano Lett.* **2013**, *13*, 1764−1769.
(35) Dualeh, A.; Tetreault, N.; Moehl, T.; Gao, P.; Nazeeruddin, M. K.; Gratzel, M. Effect of Annealing Temperature on Film Morphology of Organic-Inorganic Hybrid Pervoskite Solid-State Solar Cells. *Adv. Funct. Mater.* **2014**, *24*, 3250−3258.
(36) Tan, K. W.; Moore, D. T.; Saliba, M.; Sai, H.; Estroff, L. A.; Hanrath, T.; Snaith, H. J.; Wiesner, U. Evolution and Performance of Solar Cells. *ACS Nano* **2015**, *5*, 4730−4739.
(37) Moore, D. T.; Sai, H.; Tan, K. W.; Smilgies, D. M.; Zhang, W.; Snaith, H. J.; Wiesner, U.; Estroff, L. A. Crystallization Kinetics of Organic−Inorganic Trihalide Perovskites. *J. Am. Chem. Soc.* **2015**, *137*, 2350−2358.

DOI: 10.1021/acsami.5b02237
ACS Appl. Mater. Interfaces 2015, 7, 13440−13444